ISSN: 2447-3359

REVISTA DE GEOCIÊNCIAS DO NORDESTE

Northeast Geosciences Journal

v. 11, nº 2 (2025)

https://doi.org/10.21680/2447-3359.2025v11n2ID40118

REE-rich minerals of the Passo Feio Metacarbonatite, Dom Feliciano Belt, Brazil: microscopy and electron probe microanalysis

Minerais ricos em elementos terras raras (REE) do Metacarbonatito Passo Feio, Cinturão Dom Feliciano, Brasil: microscopia e microanálise por sonda eletrônica

Daniel Triboli Vieira[1], Edinei Koester[2], Marcelo Barcellos da Rosa[3], Lucas Mironuk[4], Delia Del Pilar Montecinos de Almeida[5], Daniel Grings Cedeño[6], Rodrigo Chaves Ramos[7], Vivianne Andrade Bastos[8], Luisa Caon[9]

[1] Institute of Geosciences, Federal University of Rio Grande do Sul - UFRGS, Porto Alegre,RS, Brazil.EMAIL: daniel.triboli@ufrgs.br
ORCID: https://orcid.org/0000-0003-0616-5407
[2] Institute of Geosciences, Federal University of Rio Grande do Sul - UFRGS, Porto Alegre, RS, Brazil. EMAIL: Koester@ufrgs.br
ORCID: https://orcid.org/0000-0002-4424-4782
[3] Department of Chemistry, Federal University of Santa Maria - UFSM, Santa Maria, RS, Brazil. EMAIL: marcelo.b.rosa@ufsm.br
ORCID: https://orcid.org/0000-0001-5959-0381;
[4] Department of Chemistry, Federal University of Santa Maria - UFSM, Santa Maria, RS, Brazil. EMAIL: lmironuk15@gmail.com
ORCID: https://orcid.org/0000-0002-7906-0254;
[5] Geology Course, Federal University of Pampa - UNIPAMPA, Caçapava do Sul, RS, Brazil**.** EMAIL: deliaalmeida@unipampa.edu.br
ORCID: https://orcid.org/0000-0002-6412-8578:
[6] Institute of Geosciences, Federal University of Rio Grande do Sul - UFRGS, Porto Alegre, RS, Brazil. EMAIL: danielgrings@tectosgeo.com
ORCID: https://orcid.org/ 0000-0001-6168-6585;
[7] Secretariat of Environment and Ecological Preservation, Municipality of Sapiranga, RS, Brazil**.** EMAIL: rodrigoramos@sapiranga.gov.rs
ORCID: https://orcid.org/0000-0001-7116-5062;
[8] Institute of Geosciences, Federal University of Rio Grande do Sul - UFRGS, Porto Alegre, RS, Brazil. EMAIL: vivianneab.vab@gmail.com
ORCID: https://orcid.org/0000-0002-4460-5285;
[9] Institute of Geosciences, Federal University of Rio Grande do Sul - UFRGS, Porto Alegre, RS, Brazil. EMAIL: luisa.caon@ufrgs.br
ORCID: https://orcid.org/0009-0002-4301-6953

Abstract: This study presents a comprehensive petrographic analysis of REE-rich minerals in the Passo Feio Metacarbonatite, located within the São Gabriel Terrane of the Dom Feliciano Belt, Brazil. The investigation employs microscopy and electron probe microanalysis to examine the mineralogical characteristics in detail. The metacarbonatite exhibits complex field relationships, marked by post-magmatic and tectonic features. It is primarily composed of calcite with subordinate dolomite, displaying granoblastic textures. Apatite and accessory minerals, including pyrochlore and monazite, serve as hosts for rare earth elements (REEs), with their compositions indicating a combination of magmatic and hydrothermal processes. Electron probe microanalysis reveals consistent compositional trends in apatite, monazite, and pyrochlore, demonstrating an enrichment in light REEs. These findings underscore the potential of the Passo Feio Metacarbonatite for REE exploration, particularly in monazite- and pyrochlore-bearing phases.

Keywords: Carbonatite; LREE; Sul-riograndense Shield.

Resumo: Este estudo oferece uma análise petrográfica detalhada dos minerais ricos em elementos terras raras (REE) encontrados no Metacarbonatito Passo Feio, situado no Terreno São Gabriel, dentro do Cinturão Dom Feliciano, Brasil. A pesquisa emprega técnicas de microscopia e microanálise por sonda eletrônica para investigar minuciosamente as características mineralógicas da rocha. O metacarbonatito apresenta relações de campo complexas, influenciadas por processos pós-magmáticos e tectônicos. Sua composição é dominada por calcita, com a presença de dolomita em menor proporção, e exibe texturas granoblásticas. Além disso, a apatita e minerais acessórios, como pirocloro e monazita, atuam como hospedeiros para os elementos de terras raras, cujas composições sugerem uma interação entre processos magmáticos e hidrotermais. As microanálises realizadas com microssonda eletrônica revelam padrões composicionais consistentes em apatita, monazita e pirocloro, evidenciando um enriquecimento em REEs leves. Esses resultados destacam o potencial do Metacarbonatito Passo Feio para a exploração de REEs, especialmente nas fases que contêm monazita e pirocloro.

Palavras-chave: Carbonatito**;** REEs leves; Escudo Sul-riograndense

Received: 06/05/2025; Accepted: 13/08/2025; Published: 21/08/2025.

1. Introduction

Light rare earth elements (LREEs) – La, Ce, Pr, Nd, Pm, Sm, and Eu – are crucial to many contemporary high-tech applications, e.g., high-efficiency magnets, luminescent materials, batteries for hybrid and electric vehicles, catalysts for oil cracking and reducing automotive emissions, special glasses, fine surface polishing, high-resistance ceramics, communication and signal amplification (detectors, radars, sonars, global positioning equipment), lasers, and weapons (Sousa Filho et al., 2019). Thus, understanding the geology of carbonatites, one of the primary natural sources of LREEs (Verplank and Van Gosen, 2016), is essential for prospecting.

The LREE enrichment of carbonatites is an inherent characteristic that arises from the melt generation mechanism, which can be either liquid immiscibility or slight partial melting of the mantle, with or without following fractional crystallization (Wang et al., 2020). The mechanisms controlling the enrichment of REEs in carbonatites can be understood by thoroughly examining their petrology. Such studies help to understand the distribution of REEs and facilitate their prospection and exploitation (Verplank and Van Gosen, 2016).

In the Sul-riograndense Shield, southern Brazil, the Passo Feio Metacarbonatite (Fig. 1) is a potential source of LREEs. Its investigation, however, presents several geological challenges since this shield has undergone multiple tectonic events and magmatic episodes over millions of years, resulting in a highly heterogeneous geological framework (Cerva-Alves et al., 2017; Morales et al., 2019). Therefore, to conduct this study on the quantification and distribution of LREEs in the Passo Feio Metacarbonatite, detailed petrography is carried out on the main host LREEs, i.e., apatite, pyrochlore, and monazite crystals, with emphasis on textural and microstructural characterization of these minerals, using optical microscopy, scanning electron microscopy (SEM), and mineral chemistry analysis (wavelength-dispersive X-ray spectroscopy - WDS) on an electron microprobe.

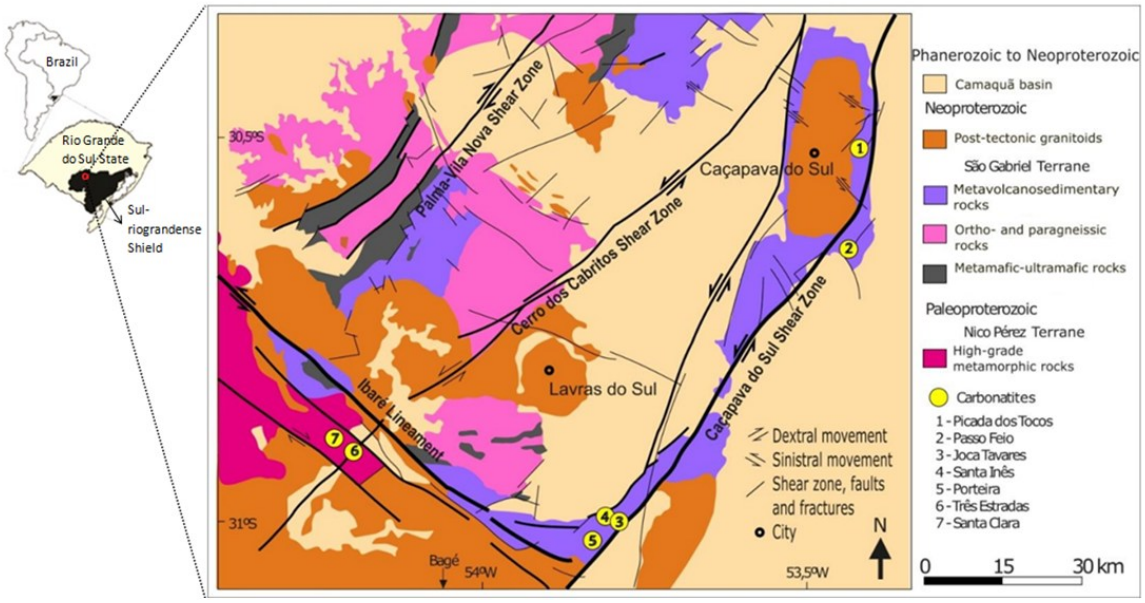

Figure 1 – Simplified geological map of the São Gabriel Terrane and the Passo Feio Complex region, highlighting the carbonatites (yellow dots).
Source: Modified from Monteiro et al. (2020).

2. Methodology

In this study, ten thin sections were prepared and analyzed at the Núcleo de Preparação de Amostras (NPA) of the Centro de Estudos em Petrologia e Geoquímica (CPGq), Instituto de Geociências (IGeo), Universidade Federal do Rio Grande do Sul (UFRGS), Brazil. Petrographic analysis and modal percentage determinations were conducted using a Leica DMLP petrographic microscope (CPGq-IGeo).

Mineral chemistry data for the primary REE-bearing minerals of the Passo Feio Metacarbonatite, including apatite, monazite, and pyrochlore, were obtained at the Electron Microscopy Laboratory of the Institut für Mineralogie,

Universität Münster, Germany, using a JEOL-8530F electron microprobe. Analytical conditions included an acceleration voltage of 15 kV and an electric current of 25 nA, with a fixed electron beam size of 5 μm for all analyses. The results demonstrated high precision for concentrations around 100 ppm, with errors below 0.1%.

Additionally, scanning electron microscopy (SEM) analyses were conducted using a JEOL-LV6400 instrument equipped with energy-dispersive spectroscopy (EDS) at the Laboratório de Geologia Isotópica (LGI), CPGq-IGeo-UFRGS. These analyses provided imaging and complementary chemical data. The EDS system was calibrated with an acceleration voltage of 15 kV and an electric current of 10 nA.

3. Results

3.1 Fieldwork and Petrography

The Passo Feio Metacarbonatite has scarce, < 1 m² outcrops, exhibiting a leucocratic rock with a fine equigranular texture. With the naked eye, it is possible to observe the presence of thin layers (approximately 2 mm thick) containing mafic minerals interspersed with calcite-rich portions.

The studied metacarbonatite exhibits intricate field relationships. No outcrops were found that show the contact relationships between the carbonatite and the rocks of the Passo Feio Complex (Fig. 2A). It displays clear evidence of post-magmatic processes linked to brittle-ductile tectonic activity, characterized by features such as folding, brecciation, and intergranular tectonic foliation, with elongated carbonate and mica crystals oriented along the foliation (Fig. 2B).

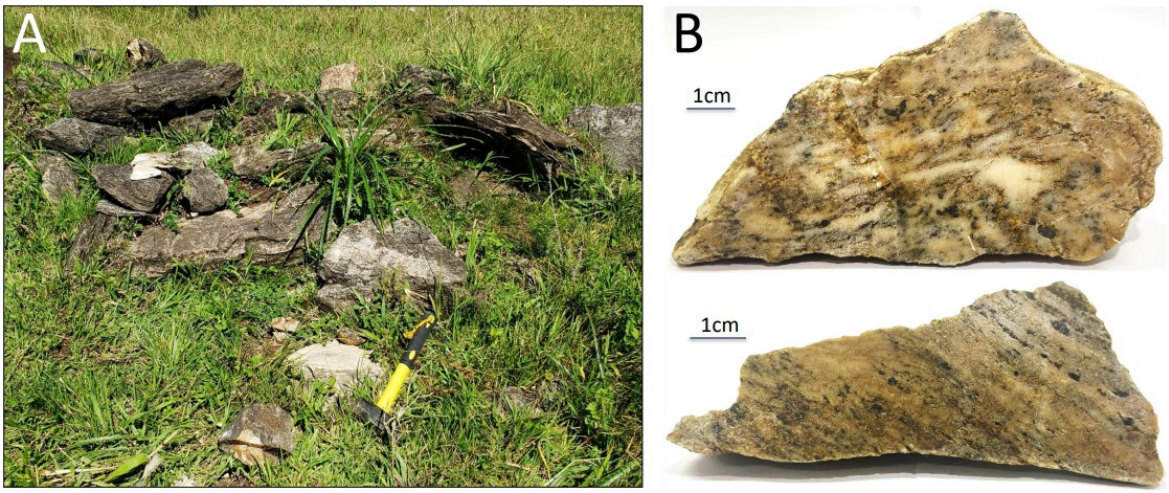

Figure 2 – Macroscopic aspects of the Passo Feio Metacarbonatite. A) Field photograph showing the exposure of the metacarbonatite in the Passo Feio region, with visible rock fragments. The hammer is 20 cm long. B) Photographs of two hand samples of the metacarbonatite, showing their texture (black arrow).
Source: Authors (2025).

The Passo Feio Metacarbonatite mainly comprises primary carbonates, calcite (70-85 modal %), and subordinate dolomite. The main carbonate occurs as subhedral calcite grains, approximately 0.4 mm in size, generally with polygonal contacts characterizing a polygonal granoblastic texture and moderate to strong undulose extinction (Fig. 3A). Dolomite occurs as tiny subhedral crystals in the interstices of the calcite crystals (Fig. 3B). The carbonates generally have inclusions of barite, zircon, and monazite and also occur as anhedral inclusions in apatite crystals (Fig. 3C). Tardimagmatic calcites occur as veins or veinlets that cut the primary carbonates (Fig. 3D, E and F).

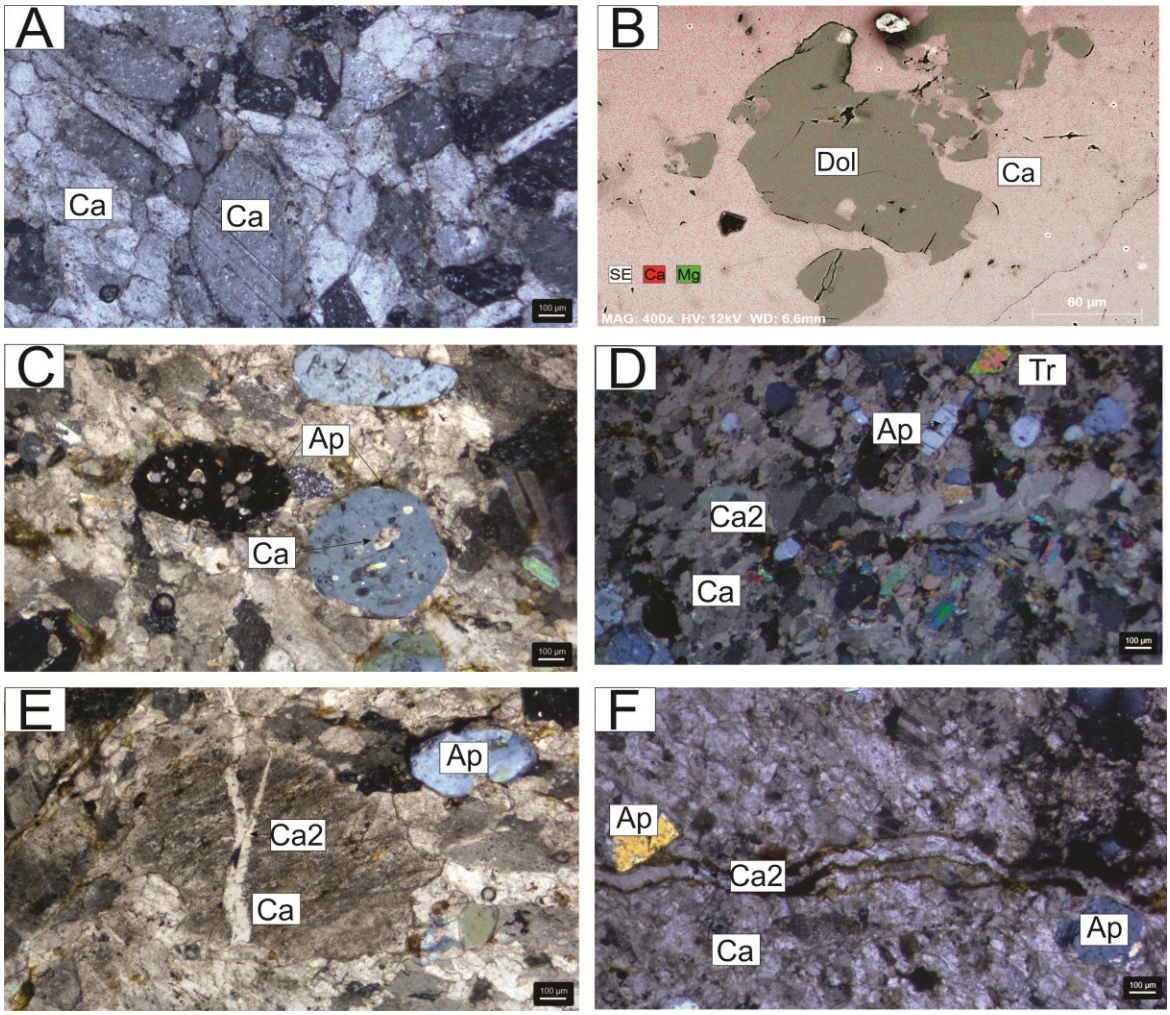

Figure 3 – Crossed-polarized photomicrographs and SEM images of the studied samples. A) Calcite crystals with polygonal textures. B) Backscattered electron image highlighting dolomite and calcite. C) Apatite crystals within a calcite. D) Apatite, calcite (primary and tardimagmatic), and tremolite, with colorful interference patterns typical of carbonate crystals. (E) Apatite and calcite crystals showing cutting relationships. (F) Close-up of apatite crystals with surrounding calcite in a finely fractured matrix, suggesting post-magmatic alteration. Abbreviations: Ap = apatite; Ca = primary calcite; Ca2 = tardimagmatic calcite; Dol = dolomite; Tr = tremolite.
Source: Authors (2025).

The apatite crystals (10-15 modal %) range from 200 to 500 µm in size. These crystals are magmatic, early formed, sometimes cut by secondary carbonates (Fig. 4A), and sometimes stretched along the mylonitic foliation (Fig. 4C). Inclusions of monazite and carbonates are common, both at the edges (Fig. 4B) and within the grain (Fig. 4D). The apatite crystals are generally prismatic, showing oscillatory zoning (Fig. 5A and 5B).

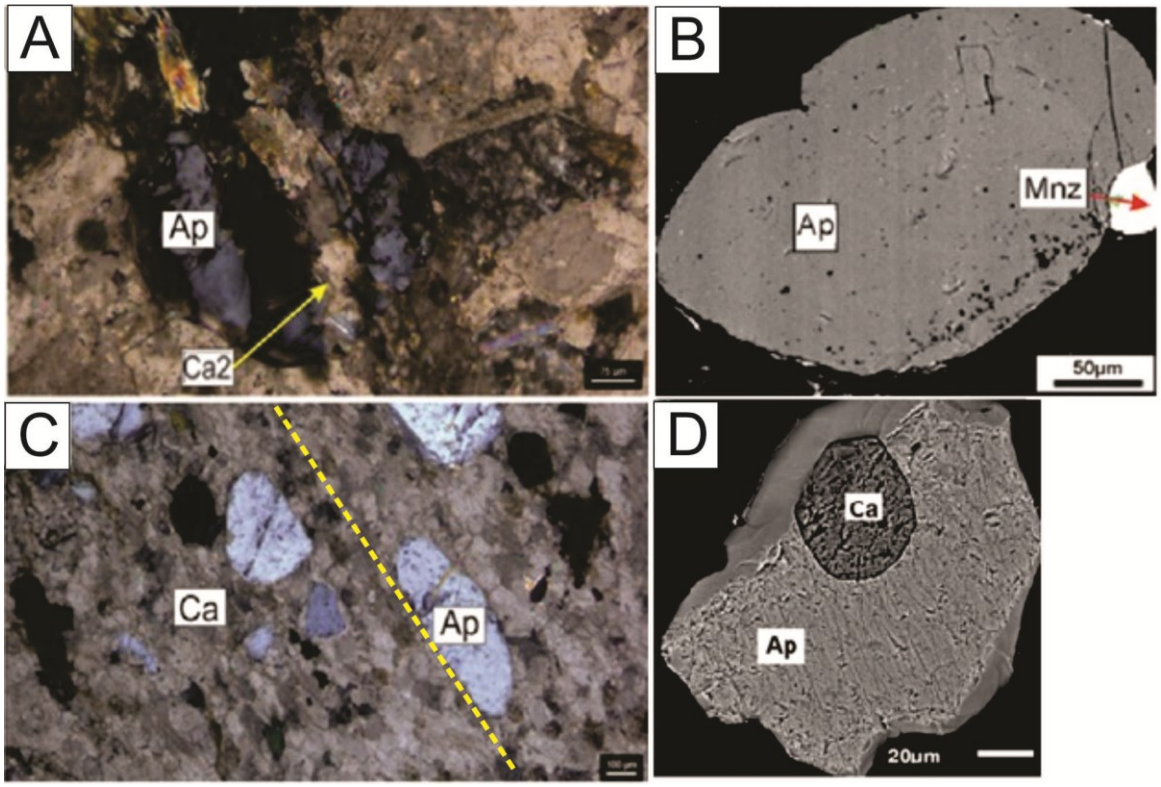

Figure 4 – Crossed-polarized photomicrographs and SEM images of the studied samples. A) Photomicrograph showing apatite and tardimagmatic calcite. B) Backscattered electron (BSE) image highlighting apatite and a monazite inclusion (red arrow). C) Photomicrograph displaying apatite and calcite grains, with a yellow dashed line indicating a tectonic foliation. D) SEM image showing the inclusion of calcite within apatite at high magnification. Abbreviations: Ap = apatite; Ca1 = primary calcite; Ca2 = tardimagmatic calcite; Mnz = monazite.
Source: Authors (2025)

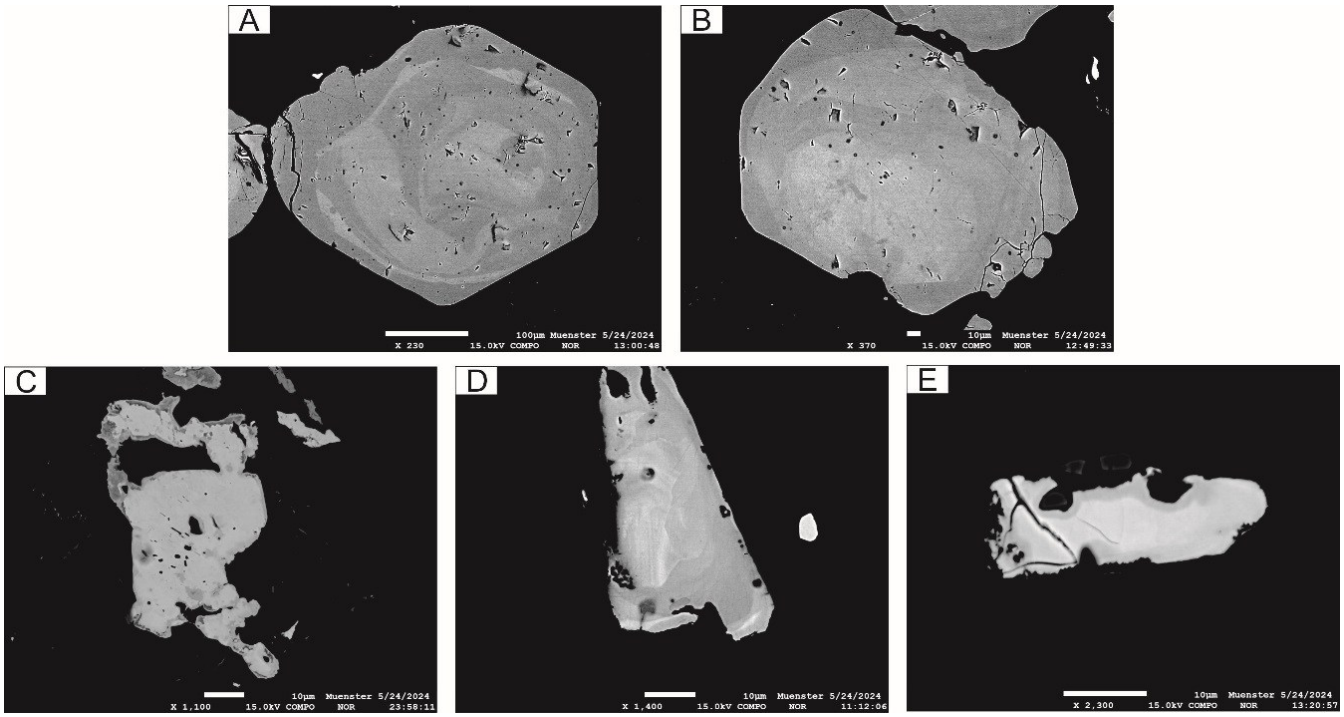

Figure 5 – Backscattered electron (BSE) images of apatite and pyrochlore crystals of the studied samples. A) Apatite grain showing oscillatory zoning. B) Apatite crystal with concentric zoning, fractures, and inclusions. C) Anhedral pyrochlore crystal with irregular boundaries; D) Pyrochlore crystal displaying compositional heterogeneity zoning; E) Pyrochlore crystal displaying corroded boundaries.
Source: Authors (2025).

The amphiboles occur as subhedral to euhedral crystals, ranging from 0.4 to 2 mm. The orientation of these crystals, together with those from phlogopite (modified to chlorite) and apatite crystals, reveals a tectonic fabric (Fig. 6A). The micas occur as subhedral porphyroblasts ranging in size from 0.5 to 3 mm. These crystals are sometimes deformed, forming kink bands (Fig. 6B). The barite occurs as anhedral crystals, often rounded, ranging in size from 0.05 to 100 mm, usually associated with carbonates.

The pyrochlore occurs as small (0.05 mm) brown to dark red subhedral crystals (Fig. 6C). These crystals occur as inclusions in apatites, disseminated crystals in the carbonate matrix, aggregates, and clusters. The pyrochlore is generally zoned and has fractures and eroded edges (Fig. 5C and 5D).

The pyrite forms euhedral crystals ranging from 0.5 to 2 mm. These crystals are often surrounded by hematite and magnetite (Fig. 6D). Zircon and monazite crystals occur as inclusions in apatites, primary carbonates, and phlogopites characterized by pleochroic haloes.

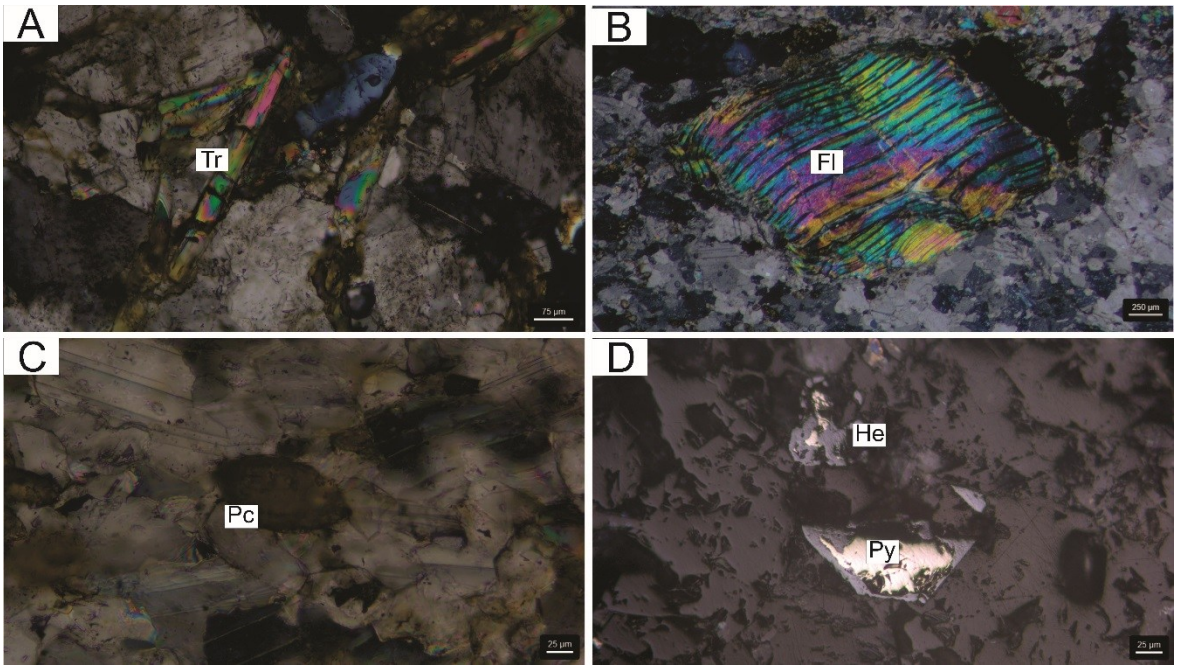

Figure 6 – Photomicrographs of the studied thin sections. A) Crossed-polarized photomicrograph displaying tremolite and calcite grains with high birefringence. B) Crossed-polarized photomicrograph showing phlogopite and calcite. C) Crossed-polarized photomicrograph highlighting pyrochlore within a calcite matrix. D) Photomicrograph showing pyrite and hematite under plane-polarized light. Abbreviation: Ca = calcite; He = hematite; Pc = pyrochlore; Phl = phlogopite; Py = pyrite; Tr = tremolite.
Source: Authors (2025).

3.2 Electron probe microanalysis (WDS)

The composition of the apatite crystals of the studied metacarbonatite is constant (Table 1), with high concentrations of P_2O_5 (up to 42.25 wt%) and CaO (up to 57.36 wt%), and minor F ranging from 1.36 to 2.67 wt%. The studied apatites are fluorapatites (Fig. 7A), typical of magmatic carbonatitic rocks (Fig. 7B and Fig. 7C).

Table 1 – Composition of apatite crystal cores (C) and rims (R) of the analysed samples.

	1		2		3		4		5	
Sample/(Wt%)	C	R	C	R	C	R	C	R	C	R
F	2.06	1.92	2.12	2.46	2.47	2.84	2.06	1.84	1.81	2.4
Na_2O	0.13	0.13	0.09	0.18	0.16	0.15	0.14	0.07	0.03	0.11
MgO	0.03	0.01	0.00	0.03	0.03	0.00	0.06	0.00	0.02	0.00
Al_2O_3	0.00	0.00	0.02	0.00	0.00	0.00	0.00	0.02	0.00	0.00
SiO_2	0.38	0.06	0.19	0.04	0.20	0.07	0.31	0.11	0.32	0.13
TiO_2	0.00	0.00	0.00	0.00	0.03	0.00	0.00	0.03	0.00	0.09
La_2O_3	0.09	0.06	0.00	0.15	0.30	0.45	0.27	0.45	0.33	0.42
Ce_2O_3	0.07	0.09	0.34	0.18	0.61	0.43	0.52	0.11	0.63	0.11
Nd_2O_3	0.32	0.12	0.50	0.00	0.36	0.00	0.02	0.09	0.09	0.06
MnO	0.00	0.00	0.03	0.03	0.03	0.03	0.00	0.04	0.03	0.02
FeO	0.54	0.26	0.00	0.00	0.05	0.04	0.02	0.05	0.03	0.00

Gd_2O_3	0.00	0.00	0.23	0.11	0.00	0.02	0.12	0.00	0.23	0.25
Yb_2O_3	0.00	0.10	0.07	0.00	0.00	0.00	0.00	0.00	0.00	0.01
SrO	0.26	0.42	0.42	0.35	0.33	0.36	0.37	0.46	0.31	0.43
ZrO_2	0.00	0.00	0.00	0.00	0.00	0.00	0.00	0.00	0.00	0.00
ThO_2	0.00	0.00	0.00	0.03	0.03	0.00	0.00	0.07	0.00	0.00
K_2O	0.00	0.00	0.00	0.00	0.00	0.00	0.00	0.00	0.00	0.00
UO_2	0.03	0.02	0.00	0.05	0.06	0.02	0.00	0.00	0.00	0.00
BaO	0.00	0.12	0.03	0.00	0.06	0.08	0.00	0.11	0.13	0.10
Ta_2O_5	0.03	0.02	0.00	0.00	0.00	0.00	0.03	0.03	0.01	0.05
Y_2O_3	0.11	0.01	0.06	0.04	0.08	0.01	0.09	0.01	0.01	0.00
P_2O_5	40.93	41.79	41.84	41.86	42.13	42.7	41.68	42.35	42.13	42.48
Nb_2O_5	0.03	0.00	0.06	0.05	0.05	0.00	0.04	0.02	0.00	0.01
SO_3	0.21	0.20	0.08	0.19	0.13	0.20	0.03	0.04	0.04	0.07
CaO	55.1	55.81	55.87	56.21	55.96	56.15	55.8	55.96	55.69	55.84
Total (Mass%)	100.95	101.14	101.95	101.96	103.07	102.53	101.56	101.87	101.93	102.31
Elem (A.P.F.U.)										
Ca	9.78	9.84	9.8	9.83	9.71	9.65	9.8	9.78	9.75	9.71
Na	0.04	0.04	0.03	0.06	0.05	0.05	0.05	0.02	0.01	0.04
Mn	0.00	0.00	0.00	0.00	0.00	0.00	0.00	0.00	0.00	0.00
Fe	0.07	0.04	0.00	0.00	0.00	0.00	0.00	0.00	0.00	0.00
La	0.01	0.00	0.00	0.01	0.02	0.03	0.02	0.03	0.02	0.01
Ce	0.04	0.01	0.02	0.01	0.04	0.03	0.03	0.01	0.04	0.01
Pr	0.00	0.00	0.00	0.01	0.00	0.00	0.01	0.00	0.00	0.00
Nd	0.02	0.01	0.03	0.00	0.02	0.00	0.00	0.01	0.01	0.00
P	5.74	5.82	5.8	5.78	5.78	5.8	5.79	5.85	5.83	5.84
Si	0.06	0.01	0.03	0.01	0.03	0.01	0.05	0.02	0.05	0.02
Cl	0.00	0.00	0.00	0.00	0.00	0.00	0.00	0.00	0.00	0.00
F	1.08	1.00	1.10	1.27	1.27	1.44	1.07	0.95	0.94	1.23
OH	0.08	0.00	0.1	0.27	0.27	0.44	0.07	0.05	0.07	0.23
Total	16.77	16.77	16.71	16.7	16.66	16.57	16.74	16.72	16.71	16.62

	6		7		8		9		10	
Sample/(Wt%)	C	R	C	R	C	R	C	R	C	R
F	2.24	1.75	2.12	2.26	1.68	1.99	2.45	2.55	1.66	2.68
Na_2O	0.15	0.15	0.14	0.17	0.14	0.16	0.09	0.06	0.16	0.21
MgO	0.01	0.03	0.01	0.01	0.04	0.04	0.00	0.01	0.02	0.03
Al_2O_3	0.00	0.00	0.01	0.00	0.00	0.01	0.01	0.00	0.00	0.00
SiO_2	0.09	0.13	0.05	0.05	0.1	0.36	0.25	0.33	0.11	0.46
TiO_2	0.13	0.01	0.06	0.00	0.02	0.00	0.03	0.00	0.04	0.01

La_2O_3	0.00	0.18	0.00	0.00	0.15	0.12	0.24	0.27	0.30	0.54
Ce_2O_3	0.45	0.38	0.34	0.43	0.18	0.59	0.25	0.50	0.50	0.79
Nd_2O_3	0.22	0.45	0.00	0.00	0.18	0.42	0.02	0.32	0.49	0.00
MnO	0.07	0.00	0.06	0.02	0.00	0.00	0.05	0.03	0.07	0.04
FeO	0.01	0.00	0.00	0.05	0.01	0.08	0.01	0.00	0.08	0.00
Gd_2O_3	0.19	0.05	0.02	0.02	0.00	0.02	0.18	0.37	0.09	0.10
Yb_2O_3	0.00	0.00	0.05	0.01	0.07	0.08	0.00	0.00	0.12	0.00
SrO	0.34	0.34	0.41	0.45	0.29	0.44	0.39	0.40	0.46	0.29
ZrO_2	0.00	0.00	0.00	0.00	0.00	0.00	0.00	0.00	0.00	0.00
ThO_2	0.00	0.01	0.01	0.00	0.02	0.10	0.01	0.00	0.00	0.00
K2O	0.00	0.00	0.00	0.00	0.00	0.00	0.00	0.00	0.00	0.00
UO_2	0.00	0.00	0.07	0.00	0.10	0.00	0.00	0.00	0.00	0.00
BaO	0.07	0.00	0.02	0.10	0.08	0.00	0.00	0.02	0.00	0.02
Ta_2O_5	0.00	0.11	0.05	0.00	0.09	0.00	0.00	0.03	0.03	0.10
Y_2O_3	0.04	0.07	0.09	0.05	0.02	0.13	0.00	0.00	0.00	0.09
P_2O_5	42.11	41.81	41.72	42.63	42.17	41.67	41.32	41.87	42.73	41.1
Nb_2O_5	0.05	0.01	0.01	0.00	0.00	0.00	0.02	0.01	0.08	0.04
SO_3	0.18	0.06	0.26	0.22	0.18	0.21	0.06	0.07	0.33	0.14
CaO	56.03	55.38	55.57	56.42	56.4	55.13	55.29	55.54	56.00	55.58
Total	102.39	100.93	101.06	102.89	101.91	101.53	100.68	102.36	103.31	102.24
Elem (A.P.F.U.)										
Ca	9.78	9.79	9.81	9.76	9.88	9.72	9.78	9.69	9.72	9.75
Na	0.05	0.05	0.04	0.05	0.04	0.05	0.03	0.02	0.05	0.07
Mn	0.01	0.01	0.01	0.00	0.00	0.00	0.01	0.00	0.01	0.01
Fe	0.00	0.00	0.00	0.01	0.00	0.01	0.00	0.00	0.01	0.00
La	0.00	0.01	0.00	0.00	0.01	0.01	0.01	0.02	0.02	0.03
Ce	0.03	0.02	0.02	0.03	0.01	0.04	0.02	0.03	0.03	0.05
Pr	0.00	0.00	0.00	0.00	0.00	0.00	0.00	0.00	0.00	0.00
Nd	0.01	0.03	0.00	0.00	0.01	0.02	0.00	0.02	0.03	0.00
P	5.81	5.84	5.82	5.83	5.84	5.8	5.77	5.77	5.86	5.70
Si	0.01	0.02	0.01	0.01	0.02	0.06	0.04	0.05	0.02	0.08
Cl	0.00	0.00	0.00	0.00	0.00	0.00	0.00	0.00	0.00	0.00
F	1.15	0.91	1.11	1.15	0.87	1.04	1.28	1.31	0.85	1.39
OH	0.15	0.09	0.11	0.15	0.13	0.04	0.28	0.31	0.15	0.39
Total	16.70	16.76	16.72	16.69	16.80	16.71	16.66	16.61	16.75	16.68

Source: Authors (2025).

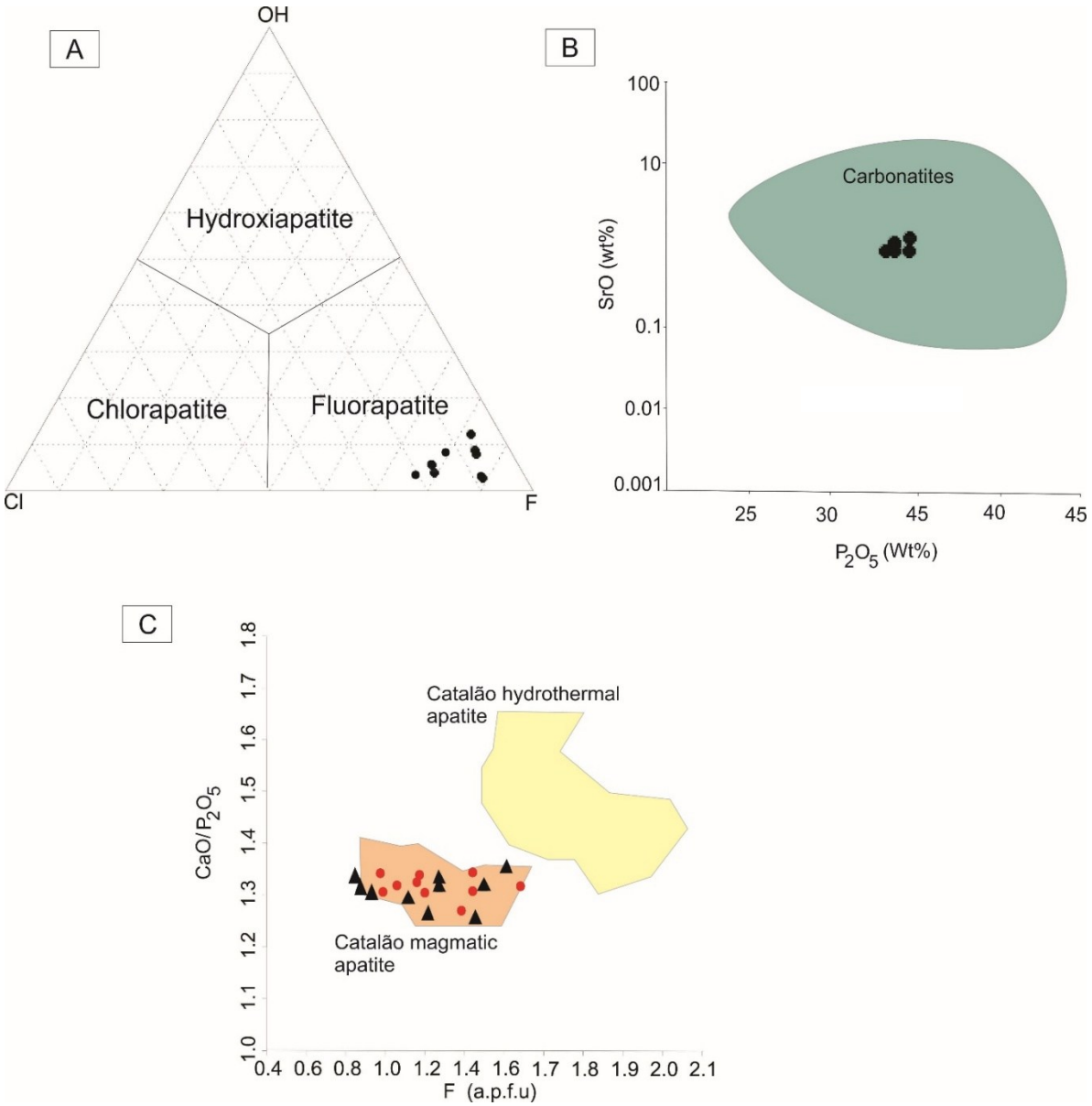

Figure 7 – Classification and composition of apatites of the studied Passo Feio Metacarbonatite samples. A) Apatite classification based on the Cl–F–OH diagram (after Patiño-Douce et al., 2011). B) P_2O_5 (wt%) vs SrO (wt%) apatite classification diagram, modified from Soltys et al. (2020); C) Distribution of the studied apatites in the CaO/P_2O_5 vs F (a.p.f.u.) diagram, showing composition within the range of magmatic and hydrothermal apatites from Catalão I (Biondi and Braga Jr., 2024). Legend: triangles = rims; circles = cores.
Source: Authors (2025).

The monazite is the main REE phosphate in the studied metacarbonatite, generally occurring in association with apatite crystals (Fig. 9A). The microanalysis results (Table 2) indicate that Ce and La are the most abundant REEs, with concentrations up to 35 (for Ce_2O_3) and 26 wt% (La_2O_3), respectively. The Nd_2O_3 concentrations range between 4 and 8 wt%. These compositions are similar to the monazites-(Ce), as shown in Figure 9B.

Table 2– Composition of monazite crystals of the analysed samples.

Sample/(Wt%)	1	2	3	4	5	6	7	8
F	0.60	0.46	0.19	0.44	0.27	0.46	0.50	0.53
Na_2O	0.00	0.00	0.00	0.00	0.00	0.00	0.00	0.00
MgO	0.00	0.01	0.00	0.00	0.00	0.00	0.00	0.00
Al_2O_3	0.02	0.00	0.00	0.00	0.00	0.00	0.02	0.00
SiO_2	0.21	0.08	0.19	0.25	0.29	0.20	0.12	0.14
TiO_2	0.12	0.03	0.00	0.00	0.00	0.00	0.11	0.04
La_2O_3	27.64	21.53	25.16	26.91	28.31	26.24	26.64	29.54
Ce_2O_3	32.82	33.92	34.3	31.97	31.84	33.99	33.44	32.26
Nd_2O_3	6.46	8.00	5.78	6.22	5.87	6.11	5.41	4.85
MnO	0.00	0.00	0.00	0.00	0.00	0.00	0.00	0.00
FeO	0.00	0.20	0.10	0.00	0.04	0.01	0.11	0.00
Gd_2O_3	0.00	0.33	0.00	0.00	0.2	0.17	0.42	0.11
$Yb2O_3$	0.00	0.22	0.05	0.00	0.02	0.00	0.10	0.00
SrO	0.15	0.00	0.10	0.02	0.13	0.11	0.07	0.10
ZrO_2	0.00	0.00	0.00	0.00	0.00	0.00	0.00	0.00
ThO_2	0.21	0.00	0.07	0.05	0.05	0.00	0.02	0.09
K_2O	0.00	0.00	0.00	0.00	0.00	0.00	0.00	0.00
UO_2	0.04	0.00	0.00	0.06	0.00	0.03	0.00	0.01
BaO	0.00	0.00	0.12	0.00	0.00	0.04	0.00	0.00
Ta_2O_5	0.00	0.00	0.00	0.00	0.00	0.16	0.10	0.06
Y_2O_3	0.00	0.000	0.08	0.00	0.00	0.13	0.10	0.00
P_2O_5	30.08	28.91	29.67	28.72	29.12	28.95	30.07	29.22
Nb_2O_5	0.00	0.01	0.00	0.06	0.00	0.00	0.05	0.05
SO_3	0.67	0.03	0.49	0.47	0.43	0.54	0.62	0.65
CaO	1.73	0.37	1.21	0.85	0.64	0.76	1.14	0.82
Total	100.73	94.08	97.5	96.01	97.23	97.92	99.05	98.48
Elem (A.P.F.U.)								
F	0.42	0.35	0.14	0.33	0.2	0.34	0.37	0.39
Na_2O	0.00	0.00	0.00	0.00	0.00	0.00	0.00	0.00
MgO	0.00	0.00	0.00	0.00	0.00	0.00	0.00	0.00
Al_2O_3	0.00	0.00	0.00	0.00	0.00	0.00	0.01	0.00
SiO_2	0.04	0.02	0.05	0.06	0.07	0.05	0.03	0.03
TiO_2	0.02	0.00	0.00	0.00	0.00	0.00	0.02	0.01
La_2O_3	2.33	1.96	2.19	2.4	2.5	2.31	2.28	2.58
Ce_2O_3	2.75	3.07	2.96	2.83	2.79	2.97	2.84	2.79
Nd_2O_3	0.52	0.71	0.49	0.54	0.50	0.52	0.45	0.41
MnO	0.00	0.00	0.00	0.00	0.00	0.00	0.00	0.00
FeO	0.00	0.04	0.02	0.00	0.01	0.00	0.02	0.00

Gd_2O_3	0.00	0.03	0.00	0.00	0.02	0.01	0.03	0.01
Yb_2O_3	0.00	0.02	0.00	0.00	0.00	0.00	0.01	0.00
SrO	0.00	0.00	0.01	0.00	0.02	0.02	0.01	0.01
ZrO_2	0.00	0.00	0.00	0.00	0.00	0.00	0.00	0.00
ThO_2	0.00	0.00	0.00	0.00	0.00	0.00	0.00	0.01
K2O	0.00	0.00	0.00	0.00	0.00	0.01	0.00	0.00
UO_2	0.00	0.00	0.00	0.00	0.00	0.00	0.00	0.00
BaO	0.00	0.00	0.01	0.00	0.00	0.00	0.00	0.00
Ta_2O_5	0.00	0.00	0.00	0.00	0.00	0.01	0.01	0.00
Y_2O_3	0.00	0.00	0.01	0.00	0.00	0.02	0.01	0.00
P_2O_5	5.84	6.05	5.92	5.89	5.89	5.85	5.92	5.85
Nb_2O_5	0.00	0.00	0.00	0.01	0.00	0.00	0.01	0.01
SO_3	0.11	0.00	0.09	0.09	0.08	0.10	0.11	0.12
CaO	0.42	0.10	0.30	0.22	0.17	0.20	0.28	0.21
Total	12.54	12.4	12.2	12.4	12.2	12.4	12.4	12.4

Source: Authors (2025).

Pyrochlore is the main REE accessory mineral in the studied metacarbonatite. Its chemical composition is variable, with significant concentrations of Nb_2O_5, TiO_2, and Ce (see Table 3). In the ternary classification diagram shown in Figure 8C, the mineral plots in the Nb = Ti > Ta group (Hogarth, 1977), and can be classified as both pyrochlore (oxycalciopyrochlore) and betafite. In the diagram shown in Figure 8D, the composition of the pyrochlore suggests a hydrothermal origin.

Table 3 – Composition of the pyrochlore crystals of the analysed samples.

Sample/(Wt %)	1	2	3	4	5	6	7	8	9	10
F	0.05	0.39	0.22	0.00	0.01	0.31	0.10	0.00	0.00	0.02
Na_2O	0.08	0.10	0.05	0.00	0.06	0.08	0.11	0.01	0.12	0.07
MgO	0.00	0.00	0.00	0.01	0.01	0.00	0.00	0.03	0.00	0.00
Al_2O_3	0.00	0.00	0.00	0.00	0.00	0.00	0.00	0.00	0.00	0.00
SiO_2	0.00	0.02	0.00	3.24	2.24	0.00	0.01	5.12	0.00	0.01
TiO_2	19.03	22.69	18.34	19.73	18.43	19.04	20.08	18.91	24.67	17.87
La_2O_3	2.66	2.74	1.55	1.49	2.24	2.38	0.87	1.68	4.82	2.94
Ce_2O_3	7.81	9.16	7.21	7.92	7.53	10.6	7.23	7.66	14.78	8.59
Nd_2O_3	4.69	5.75	4.29	5.32	5.15	5.96	8.75	4.41	8.17	5.86
MnO	0.08	0.00	0.07	0.03	0.06	0.10	0.14	0.04	0.00	0.01
FeO	3.79	3.69	3.95	3.43	3.31	3.38	3.92	2.22	2.43	3.93
Gd_2O_3	0.53	0.29	0.29	0.58	0.26	0.42	2.01	0.15	0.43	0.28

Yb_2O_3	0.00	0.01	0.00	0.00	0.00	0.00	0.06	0.00	0.00	0.00
SrO	0.05	0.13	0.17	0.16	0.16	0.13	0.00	0.27	0.00	0.09
ZrO_2	0.06	0.08	0.00	0.04	0.00	0.08	0.06	0.17	0.01	0.05
ThO_2	11.41	13.9	13.08	12.8	9.50	7.99	5.90	10.50	3.81	8.57
K_2O	0.00	0.00	0.01	0.03	0.00	0.01	0.00	0.11	0.01	0.00
UO_2	0.31	0.33	0.39	0.41	0.18	0.31	0.52	2.09	0.30	0.14
BaO	0.00	0.00	0.11	0.00	0.00	0.00	0.15	0.09	0.13	0.00
Ta_2O_5	1.35	0.88	0.96	1.04	1.90	1.90	1.87	2.53	2.65	2.42
Y_2O_3	0.38	0.3	0.34	0.36	0.23	0.29	2.11	0.27	0.45	0.23
P_2O_5	0.01	0.01	0.01	0.06	0.03	0.00	0.00	0.03	0.00	0.01
Nb_2O_5	36.91	30.5	36.26	31.31	34.95	34.76	31.94	32.35	26.18	37.93
SO_3	0.00	0.04	0.05	0.02	0.06	0.03	0.01	0.11	0.00	0.05
CaO	7.00	5.28	7.53	5.91	6.78	5.99	4.17	3.74	2.76	6.75
Total	96.2	96.3	94.87	93.7	93.1	93.75	90.00	92.59	91.71	95.82
$[H_2O(calc.)](wt.)$	0.27	0.30	0.30	0.36	0.36	0.38	0.38	0.47	0.38	0.30
Elem (A.P.F.U.)										
U	0.00	0.00	0.00	0.00	0.00	0.00	0.02	0.00	0.025	0.00
Th	0.15	0.18	0.18	0.16	0.12	0.09	0.13	0.07	0.13	0.07
La	0.04	0.04	0.02	0.02	0.04	0.04	0.02	0.00	0.02	0.09
Ce	0.15	0.20	0.16	0.15	0.15	0.22	0.15	0.16	0.14	0.33
Pr	0.00	0.00	0.00	0.00	0.00	0.00	0.00	0.00	0.00	0.00
Nd	0.08	0.11	0.09	0.106	0.11	0.11	0.09	0.18	0.08	0.17
Gd	0.00	0.00	0.00	0.00	0.00	0.00	0.00	0.04	0.00	0.00
Yb	0.00	0.00	0.00	0.00	0.00	0.00	0.00	0.03	0.00	0.00
Ca	0.45	0.33	0.47	0.32	0.38	0.33	0.32	0.27	0.18	0.13
Vacancy	1.11	1.13	1.08	1.24	1.19	1.18	1.25	1.23	1.41	1.20
Total (a.p.f.u.)	2	2	2	2	2	2	2	2	2	2
Especies	Pyrochlore group Oxycalciopyrochlore	Betafite group Not classified	Pyrochlore group Oxycalciopyrochlore	Betafite group Not classified	Pyrochlore group Oxycalciopyrochlore	Pyrochlore group Oxycalciopyrochlore	Pyrochlore group Oxycalciopyrochlore	Betafite group Not classified	Pyrochlore group Oxycalciopyrochlore	Betafite group Not classified

Source: Authors (2025).

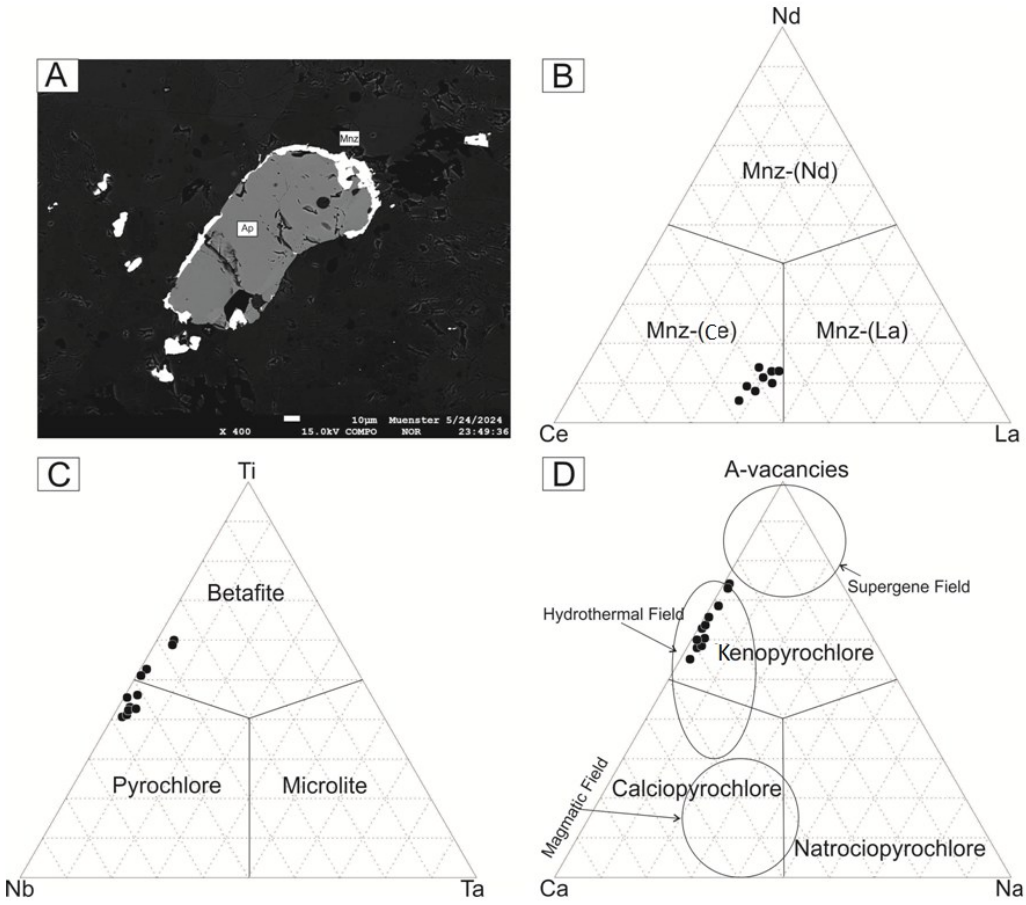

Figure 8 – SEM image of apatite, monazite, and pyrochlore ternary classification diagrams for Passo Feio Metacarbonatite. A) SEM image of an apatite (Ap) crystal surrounded by a rim of monazite (Mnz). B) Compositional variability of monazite (Mnz) in terms of Ce, La, and Nd content (modified by Nickel, 1992). C) Classification of pyrochlore group minerals based on Nb, Ta, and Ti proportions (modified by Finch et al., 2019). D) Classification of pyrochlore group minerals in terms of Ca, Na, and A-site vacancies (modified by Zurevinski et al., 2004), highlighting fields of magmatic, hydrothermal, and supergene processes. Black dots represent the analyzed samples.
Source: Authors (2025).

4. Discussion

According to the classification of Le Maitre et al. (2002), the Passo Feio Metacarbonatite is an alkivite characterized by its medium-grained texture and calciocarbonatitic composition, i.e., with a predominance of calcite over dolomite. The presence of late magmatic carbonates may be attributed to the percolation of hydrothermal fluids, which are likely a consequence of deformational tectonics and granitic intrusions, as suggested by Cerva-Alves et al. (2017) and Morales et al. (2019).

Regarding the mineralogical composition of the studied metacarbonatite, apatite is one of the main minerals, constituting approximately 17 wt% of the analyzed samples. According to Chakhmouradian et al. (2017), apatite is a critical phase in regulating the variations of P and REEs within carbonatites, offering insights into mineral-fluid interactions. The CaO/P_2O_5 ratios of the analysed apatites, ranging from 1.27 to 1.31, along with SrO concentrations < 1

wt%, indicate that these minerals have likely experienced interactions with hydrothermal fluids (Chakhmouradian et al., 2017).

Chakhmouradian et al. (2017) further assert that igneous apatites typically exhibit enrichment of REEs from core to rim, aligning with the observed Ce, La, and Nd values in the examined samples. The apatites in the present study display oscillatory zoning (Fig. 5A and 5B) with a slight enrichment of LREEs from core to rim (Table 1), particularly for Ce, La, and Nd. This pattern indicates apatites formed in strongly alkaline environments (Chakhmouradian et al. 2017). Consequently, the studied apatites are mostly igneous, originated from an alkaline environment, similar to those of the Alto Paranaíba Igneous Province (Fig 7.C)

In the context of potential cation exchanges within apatite crystals (Toledo and Pereira, 2001), particular emphasis is placed on those involving REEs, owing to their crucial role in elucidating the chemical evolution of the parental magmas of carbonatites. Despite the apatite compositional exhibited by these rocks, REEs demonstrate compatibility with apatite crystals within these systems (Chakhmouradian et al., 2017). Notably, these elements are also compatible with a wide range of minerals that may co-precipitate with apatites, consequently influencing the chemical evolution of the latter mineral due to the extraction of elements that would otherwise be fully integrated into its crystalline structure. Thus, the formation of REE-depleted apatite crystals is expected, followed by the formation of other minerals enriched in these elements, such as monazites (Chakhmouradian et al., 2017), as exemplified in the case of the studied metacarbonatite.

The association between monazite and apatite is frequently observed across various rock types. It has been attributed to magmatic crystallization (Wark and Miller, 1993) or processes involving apatite-hydrothermal fluid reactions (Harlov, 2015). Specifically, the monazite formed within a carbonatite may result from interactions between CO_2-rich fluids and apatite crystals (Harlov, 2015). In this process, LREEs are leached from the apatite, increasing the concentration of these elements in the anhedral monazite crystals at the apatite's edges (see Figs. 5B, 8A).

The genesis of monazite from apatite implies that this mineral uses the P_2O_4-tetrahedra resulting from the breakdown of apatite, thereby facilitating monazite growth at the edges of the apatite crystals. The study of Finger et al. (1998) indicates that this substitution reaction initiates with the opening of the apatite around 350°C, which aligns with the formation temperatures of the microstructures observed in the studied metacarbonatite as calcites underwent dynamic recrystallization, resulting in a polygonal granoblastic texture and the formation of kink bands in the phlogopites (Figs. 3A, 6B). Kennedy and White (2001) reported dynamic calcite and mica deformation recrystallization at temperatures ranging from 150 to 450 °C.

The analyzed monazite samples exhibit high concentrations of LREEs, with a predominance of Ce, followed by La and Nd. These samples were characterized as monazites-(Ce). According to Chakhmouradian et al. (2017), the gradual concentration and enrichment in LREEs, particularly Ce^{3+} and La^{3+}, is indicative of phosphates generated in strongly alkaline conditions, where $LREE^{3+}$ most likely substitutes Ca^{2+} during the magma crystallization.

Additional features observed in the studied metacarbonatite include the formation of a secondary carbonate phase that occurs as veins and veinlets discordant with the tectonic foliations (Fig. 3D, 3E, and 3F). Furthermore, there is evidence of comminution at the edges of the pyrochlores, followed by fracturing (Fig. 5D, 5E, and 5F).

In the Ti vs Nb vs Ta classification diagram shown in Figure 8B, the studied pyrochlores plot into the pyrochlore and betafite groups. The analysed pyrochlores are often rich in REE (up to 20.4 wt% REE oxides), Th (up to 13.9 wt% ThO_2), and U (up to 0.2 wt% UO_2) but low in Ba, similar to the ceriopyrochlores of Hogarth (1977).

Pyrochlore samples exhibit irregular zonation, corroded rims, and metamictization halos (Figs. 5C, 5D and 5E), which are typical of pyrochlores generated in hydrothermal environments (Xue et al., 2021), supporting the Zurevinsk and Mitchell (2004) classification (Fig. 8D). According to Lumpkin and Ewing (1995) and Wall et al. (1996), A-site vacancies in the pyrochlore formula distinguish fractured and partially corroded pyrochlores typical of late hydrothermal alteration and weathering (Biondi and Braga Jr., 2024). Regarding the studied pyrochlores, these crystals exhibit considerable A-site vacancies, depletion in Na-Ca-Si-Al, and enrichment in REEs and Ti, typical of pyrochlores with high A-site vacancies caused by hydrothermal alteration (Lumpkin and Ewing, 1992).

According to Morales et al. (2019), a whole rock geochemistry study, the Passo Feio Metacarbonatite shows an enrichment in LREEs relative to HREEs, likely due to a concentration of LREE-rich minerals. Thus, the mineral chemistry study presented here corroborates this hypothesis due to the observed LREE-rich composition of the studied monazites, pyrochlores, and apatites.

Morales et al. (2019) and Campestrini et al. (2024) noted that the LREE concentrations of the Passo Feio Metacarbonatite are within the standards established in the literature for this group of rocks (Fig. 9A). In REE chondrite-normalized diagrams (Morales et al., 2019) the Passo Feio Metacarbonatite shows a pattern similar to that found in

carbonatites from the Alto Paranaíba Igneous Province (Gomide et al., 2016) and Lages Alkaline Complex (Gomes et al., 2018), two relevant REE-rich sites in Brazil (Fig. 9B).

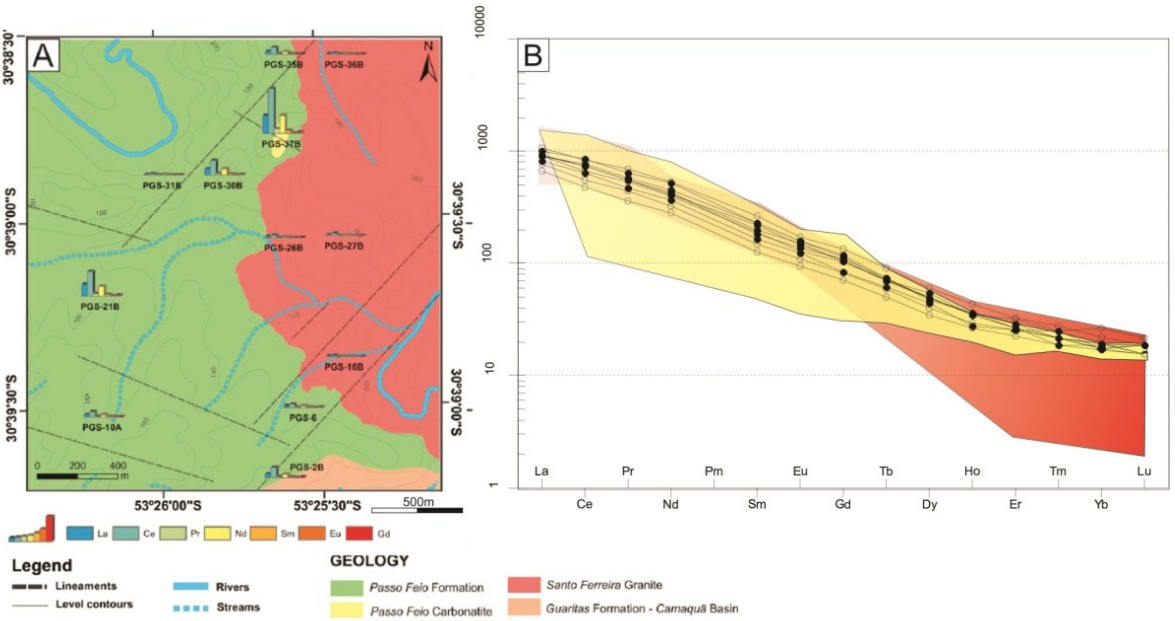

Figure 9 – Geochemical characteristics of the Passo Feio Metacarbonatite, based on previous studies. A) Simplified geological map of the study area, highlighting the distribution of LREE, modified by Morales et al. (2019). B) Chondrite-normalized (Boynton, 1984) whole rock REE signatures of the studied metacarbonatite. Legend: Black dots = samples of Morales et al. (2019); White dots = samples of Campestrini et al. (2024). Yellow Field = Lages Carbonatite (Gomes et al., 2018); Red field = carbonatites from Alto Paranaíba Igneous Province (Gomide et al., 2016).
Source: Authors (2025).

The metamorphic and hydrothermal processes are also evidenced in the studied metacarbonatite by its $^{13}\delta C_{V\text{-}PDB}$ and $^{18}\delta O_{SMOW}$ stable isotopic signatures (Morales et al., 2019), which indicate the occurrence of metamorphic deformational processes due to its displacement from the igneous field. The latter feature can be explained by the process described by Demény et al. (2006), in which this isotopic variation can result from both deformational and hydrothermal processes. Thus, based on the petrographic evidence and the relatively low variation of $^{18}\delta O_{SMOW}$, it is possible to suggest the occurrence of both metamorphic and hydrothermal processes. It is likely that during these processes, a large portion of the primary calcites underwent dynamic recrystallization, resulting in a polygonal granoblastic texture and the formation of kink bands in the phlogopites.

5. Concluding remarks

The Passo Feio Metacarbonatite is a primary alkivite. The studied rock presents small carbonate portions represented by veins and veinlets, possibly resulting from the percolation of hydrothermal fluids caused by tectonic stresses, as evidenced by deformational structures formed around 450 °C.

Regarding REE distribution, the studied metacarbonatite is rich in LREEs (particularly La and Ce), predominantly concentrated in the main mineral apatite and accessory mineral phases such as monazite and pyrochlore, formed through hydrothermal processes. Although apatites have a relatively low LREE concentration, they account for more than 16 % of the rock's composition.

Acknowledgments

The authors acknowledge the Instituto de Geociências of UFRGS for technical and infrastructure support. Additionally, we recognize Conselho Nacional de Desenvolvimento Científico e Tecnológico (CNPq) and Fundação de Amparo à Pesquisa do Estado do RS (FAPERGS) for financial support.

References

Biondi, J.C., Braga Jr, J.M. Main minerals of the Araxá alkali-carbonatite complex, Minas Gerais State, Brazil. *Journal of South American Earth Sciences*, 134, 104751, 2024.

Boynton, W.V. Cosmochemistry of the rare earth elements: meteorite studies. In *Developments in geochemistry* (Vol. 2, pp. 63-114). Elsevier. 1984.

Campestrini, G.N., Rosa, M.B., Vieira, D.T., Koester, E., Almeida, M.D., Porcher, C.C., Dubbon, I.G., Correa, V.C., Mironuk, L., Ramos, R.C., Amorim, A.F. *Geoquímica do Metacarbonatito Passo Feio, Caçapava do Sul, RS: contribuições para a pesquisa de ETR*. In: CONGRESSO BRASILEIRO DE GEOLOGIA, 51, 2024, Belo Horizonte. Anais... Belo Horizonte, SBG, 1150, 2024.

Cerva-Alves, T., Remus, M.V.D., Dani N., Basei, M.A.S. Integrated field, mineralogical and geochemical characteristics of Caçapava do Sul alvikite and beforsite intrusions: A new Ediacaran carbonatite complex in southernmost Brazil. *Ore Geology Reviews*, 88:352-369. DOI: 10.1016/j.oregeorev. 2017.

Chakhmouradian, A., Reguir, E., Zaitsev, A., Coueslan, C., Xu, C., Kynicky, J., Mumin, A., Yang, P. Apatite in carbonatitic rocks: Compositional variation, zoning, element partitioning and petrogenetic significance. *Lithos*, 274, 188-213. 2017.

Demény, A., Sitnikova, M.A., Karchevsky, P.I. Stable C and O isotope compositions of carbonatite complexes of the Kola Alkaline Province: phoscorite-carbonatite relationships and source compositions. *Mineralogy Society of Serbia*. 10. 2006.

Finch, A.A., McCreath, J.A., Reekie, C.D.J., Hutchison, W., Ismaila, A., Armour, B.A., Andersen, T., Simonsen, S.L. From mantle to Motzfeldt: A genetic model for syenite-hosted Ta Nb-mineralization. *Ore Geology Review*, 107, 402–416. 2019.

Finger, F., Broska, I., Roberts, M.P., Schermaier, A. Replacement of primary monazite by apatite – allanite – epidote coronas in an amphibolite facies granite gneiss from the eastern Alps. *American Mineralogist*, 83, 248-258. 1998.

Gomes, C. D. B., Comin-Chiaramonti, P., Azzone, R. G., Ruberti, E., & Rojas, G. E. E. Cretaceous carbonatites of the southeastern Brazilian Platform: a review. *Brazilian Journal of Geology*, *48*, 317-345. 2018.

Gomide, C. S., Brod, J. A., Vieira, L. C., Junqueira-Brod, T. C., Petrinovic, I. A., Santos, R. V., Mancini, L. H. Stable (C, O, S) isotopes and whole-rock geochemistry of carbonatites from Alto Paranaíba Igneous Province, SE Brazil. *Brazilian Journal of Geology*, *46*(03), 351-376. 2016.

Harlov D.E. Apatite: A Fingerprint for Metasomatic Processes. *Elements* 11, 171-176. 637. 2015.

Hogarth, D.D. Classification and nomenclature of the pyrochlore group. *American Mineralogist*, 62, 403-410.1977.

Kennedy, L.A., White, J.C. Low-temperature recrystallization in calcite: Mechanisms and consequences. *Geology*, *29*(11), 1027-1030. 2001.

Le Maitre, R.W., Streckeisen, A., Zanettin, B., Le Bas, M.J., Bonin, B., Bateman, P. (eds). Frontmatter. In: *Igneous Rocks: A Classification and Glossary of Terms: Recommendations of the International Union of Geological Sciences Subcommission on the Systematics of Igneous Rocks*. Cambridge University Press; 2002: i-iv. 2002.

Lumpkin G.R., Ewing C.R. Geochemical alteration of pyrochlore group minerals: microlite subgroup. *American Mineralogist,* 77, 179-188. 1992.

Lumpkin G.R., Ewing C.R. Geochemical alteration of pyrochlore group minerals: pyrochlore subgroup. *American Mineralogist*, 80, 732-743. 1995.

Monteiro, C. F., de Oliveira, I. L., Brod, J. A., Dantas, E. L., de Araujo, C. E. G., Zacchi, É. N. P., Fuck, R. A., Nd-Sr-Hf isotopes and U-Pb ages of mesoproterozoic Três Estradas Alkaline-Carbonatite Complex, Brazil: Implications for Sul-Riograndense Shield evolution and Rodinia break-up. *Precambrian Research*, 351, 105963. 2020.

Morales, B.A.A., Almeida, D.P.M., Koester, E., Rocha, A.M.R., Dorneles, N.T., Rosa, M.B., Martins, A.A. Mineralogy, whole-rock geochemistry and C, O isotopes from Passo Feio Carbonatite, Sul-Riograndense Shield, Brazil. *Journal of South American Earth Sciences*, 94, 102-208. DOI: 10.1016/j.jsames.2019.05.024. 2019.

Nickel E.H. Solid solutions in mineral nomenclature. *Mineralogy and Petrology*, 46(1), 49-53. 1992.

Patino-Douce, A.E., Roden, M., Chaumba, J., Fleisher, C., Yogodzinski, G., Compositional variability of terrestrial mantle apatites, thermodynamic modeling of apatite volatile contents, and the halogen and water budgets of planetary mantles. *Chemical Geology*, 288, 14–31. 2011.

Siegesmund, S., Basei, M.A.S., Oyhantçabal, P., Oriolo, S. (Eds.). Geology of Southwest Gondwana. Springer, *Regional Geology Reviews*, 688p. 2018.

Soltys, A., Giuliani, A., Phillips, D. Apatite compositions and groundmass mineralogy record divergent melt/fluid evolution trajectories in coherent kimberlites caused by differing emplacement mechanisms. *Contributions to Mineralogy and Petrology*, 175, 1–20. 2020.

Sousa Filho, P.C., Galaço, A.R.B.S., Serra, O.A. Terras Raras: tabela periódica, descobrimento, exploração no Brasil e aplicações. *Quimica Nova*, 42(10), 1208-1224. 2019.

Toledo, M.C.M., Pereira, V.P. Variabilidade de composição da apatita associada a carbonatitos. *Revista do Instituto Geológico*, 22 (1/1), 27-64. 2001.

Verplank, P.L., Mariano, A.N. Rare earth element ore geology of carbonatites. *Economic Geology Society*, 18, 5–32. 2016.

Wall, F., William, C.T., Woolley, A.R., Nasraqui, M., Pyrochlore from weathered carbonatite at Lueshe, Zaire. *Mineralogical Magazine*, 60, 731-750. 1996.

Wang, Z.Y. et al. Carbonatite-related REE deposits: An overview. *Minerals*, 10, 1-26. 2020.

Wark, D., Miller, A., Calvin F. Accessory mineral behavior during differentiation of a granite suite: monazite, xenotime and zircon in the Sweetwater Wash pluton, southeastern California, U.S.A. Chemical Geology, 110(1), 49-67. 1993.

Xue, Y., Sun, N., Li, G. Evolution of Nb–Ta Oxide Minerals and Their Relationship to the Magmatic-Hydrothermal Processes of the Nb–Ta Mineralized Syenitic Dikes in the Panxi Region, SW China. *Minerals*, *11*, 1204. 2021.

Zurevinski, S.E., Mitchell, R.H. Extreme compositional variation of pyrochlore-group minerals at the Oka carbonatite complex, Quebec: evidence of magma mixing? *Canadian Mineralogy*, 42, 1159e1168. 2004.